International Journal of Pharmaceutics 421 (2011) 72–81

Contents lists available at SciVerse ScienceDirect

International Journal of Pharmaceutics

journal homepage: www.elsevier.com/locate/ijpharm

The kinetics of cohesive powder de-agglomeration from three inhaler devices

Srinivas Ravindra Babu Behara[a], Ian Larson[a], Paul Kippax[b], David A.V. Morton[a], Peter Stewart[a,*]

[a] Drug Delivery, Disposition and Dynamics, Monash Institute of Pharmaceutical Sciences, Monash University, 381 Royal Parade, Parkville, Victoria 3052, Australia
[b] Malvern Instruments, Enigma Business Park, Grovewood Road, Malvern, Worcestershire WR14 1XZ, UK

ARTICLE INFO

Article history:
Received 26 May 2011
Received in revised form 20 August 2011
Accepted 19 September 2011
Available online 21 September 2011

Keywords:
Dry powder inhaler
De-agglomeration
Kinetics
Laser diffraction
Non-linear regression modelling

ABSTRACT

Purpose: The purpose of the current investigation is to understand the kinetics of de-agglomeration (k_d) of micronised salbutamol sulphate (SS) and lactohale 300 (LH300) under varying air flow rates (30–180 l min^{-1}) from three dry powder inhaler devices (DPIs), Rotahaler® (RH), Monodose Inhaler® (MI) and Handihaler® (HH).
Results: Cumulative fine particle mass *vs.* time profiles were obtained from the powder concentration, emitted mass and volume percent <5.4 μm, embedded in the particle size distributions of the aerosol at specific times. The rate of de-agglomeration (k_d), estimated from non-linear least squares modelling, increased with increasing air flow rates. The k_d *vs.* air flow rate profiles of SS and LH300 were significantly different at high air flow rates. The k_d was highest from RH and lowest from MI. Differences in k_d between the devices were related to device mode of operation while the differences between the materials were due to the powder bed structure.
Conclusion: This approach provided a methodology to measure the rate constant for cohesive powder de-agglomeration following aerosolisation from commercial devices and an initial understanding of the influence of device, air flow rate and material on these rate constants.

1. Introduction

The regulatory concern on ozone depleting effect of chlorofluorocarbons used in pressurized metered dose inhalers has accelerated the development of dry powder inhalation technology. The key challenge in dry powder inhalation is to generate fine particles which can deposit in the lower respiratory tract. However, these micronised fine particles are cohesive because the magnitude of gravitational forces is much less than interactive forces (Visser, 1989). In order to improve the de-agglomeration efficiencies in powders for inhalation, consideration needs to be given to factors relating both to the cohesive powder structure and to the device design.

The cohesive powder tensile strength is defined by its particle size, work of cohesion or adhesion and packing fraction (Kendall and Stainton, 2001). As the extent of de-agglomeration is related to tensile strength, aerosolisation of cohesive powders for inhalation can be manipulated by optimising work of cohesion/adhesion and packing fraction, since the particle size is fixed by functionality. The de-agglomeration behaviour of powders will therefore be determined by the structure of the powder including the distribution of particle size, particle interactions and packing fractions in the powder bed. Such behaviour has recently been seen in a study (Behara et al., 2011c) on single component systems [salbutamol sulphate (SS) and lactohale 300 (LH300)] and binary mixtures of SS and LH300 (Behara et al., 2011b). Powders (Behara et al., 2011c) were aerosolised using Rotahaler® (RH) over a range of air flow rates (30–180 l min^{-1}) to construct relative de-agglomeration *vs.* air flow rate profiles. These profiles were modelled to estimate sigmoidal parameter to characterise cohesive powders. The relative de-agglomeration increased with increases in air flow rate for SS over the whole air flow rate range, while no significant increase in de-agglomeration was observed from 90 to 180 l min^{-1} with LH300. The powder micro-structure determined the de-agglomeration behaviour and this approach was able to distinguish between powders with dispersible and non-dispersible agglomerates.

Device related de-agglomeration will be associated with the cohesive powder–capsule processes and with the cohesive powder–device interactions. Recent studies demonstrated that the de-agglomeration associated with the capsule depended on capsule aperture size (Coates et al., 2005b; Chew et al., 2002) and de-agglomeration associated with the device design will depend on grid structure (Coates et al., 2004b), mouth piece length (Coates

Abbreviations: AIC, akaike information criteria; AL, Aerolizer®; BERM, bi-exponential rise to maximum; CFPM, cumulative fine particle mass; $CFPM_{max}$, maximum cumulative fine particle mass; $CFPM_t$, cumulative fine particle mass at time "*t*"; DH, Dinkihaler®; EM_t, emitted mass at time "*t*"; FPM_t, fine particle mass at time "*t*"; HH, Handihaler®; k_d, rate constant for de-agglomeration; LH300, lactohale 300; MERM, mono-exponential rise to maximum; MI, Monodose Inhaler®; RH, Rotahaler®; SS, salbutamol sulphate.

* Corresponding author. Tel.: +61 3 99039517; fax: +61 3 99039583.
E-mail address: peter.stewart@monash.edu (P. Stewart).

0378-5173/$ – see front matter © 2011 Elsevier B.V. All rights reserved.
doi:10.1016/j.ijpharm.2011.09.024

et al., 2004b), air inlet size (Coates et al., 2006) and resistance of the device (Srichana et al., 1998; Steckel and Muller, 1997).

The studies on the role of capsules on powder inhaler performance [Aerolizer® (AL)] (Coates et al., 2005b) demonstrated increased in vitro performance with decreased size of the capsule aperture using size 3 capsule. In addition, the study demonstrated that the in vitro performance primarily depended on the size of the capsule aperture rather than the total aperture area. Decrease in capsule aperture size led to increased shear on the agglomerates, where smaller apertures prevented larger agglomerates from escaping (Coates et al., 2005b) resulting in higher in vitro performance. The study by Coates et al. (2005b) were with a single inhaler device, AL which has similar device design (except inhalation port length and capsule aperture area) and mechanism of fluidization to that of Monodose Inhaler® (MI). A comparative study between devices (Chew et al., 2002), RH and Dinkihaler® (DH) (similar mechanism of fluidization as MI) concluded that the higher in vitro performance of DH at a given air flow was due to its greater resistance and higher pressure drop compared to RH. The in vitro performance *vs.* aerosolisation energy profiles showed that the higher in vitro performance of DH compared to RH at the same aerosolisation energy was due to enhanced collisions of the powder within DH caused by tangential air entrainment (Chew et al., 2002).

The effect of grid structure on the in vitro performance of AL at 60 l min^{-1} was studied using three different grid structures (Coates et al., 2004b). The study demonstrated that the in vitro performance referenced to the loaded dose decreased with increase in grid voidage. However, increased grid voidage increased powder retention in the device especially around the mouth piece. This study concluded that in vitro performance was related to the balance between particle-grid impactions causing de-agglomeration and particle-mouth piece impactions causing retention. In a comparative study between RH and AL at 60 l min^{-1}, with and without grids (Coates et al., 2004a), the presence/absence of grid had no effect on overall turbulent kinetic energies. However, the study demonstrated higher in vitro performance of AL compared to RH with and without the grid as a result of higher turbulent kinetic energy of the former. This outcome was also supported by investigation of Voss and Finlay (2002) where it was reported that the turbulence may be one of the effective de-agglomeration mechanisms and that the mechanical impaction on the rig was less significant. However, the previous study (Coates et al., 2004a) concluded that the improved de-agglomeration of grid case compared to no-grid case was due to mechanical impaction of agglomerates on the grid. Therefore both the turbulent kinetic energy and mechanical impactions are likely to contribute to powder de-agglomeration.

The effect of the length of inhaler mouth piece (Coates et al., 2004b) 0.5 and 0.75 of original length and original inhaler mouth piece length was evaluated for the powders aerosolised at 60 l min^{-1} using AL. The decrease in mouth piece length decreased the device powder retention. However, the in vitro performance (referenced against loaded and emitted doses) was least affected by inhaler mouth piece length due to similar levels of turbulence.

The air inlet size role on in vitro performance of AL between 30 and 90 l min^{-1} was investigated (Coates et al., 2006). This study used full air inlet size of AL along with and 0.33 and 0.67 of full air inlet sizes leading to device resistances of 0.072, 0.100 and 0.148 $(cmH_2O)^{1/2}$ $(l\,min^{-1})^{-1}$ respectively. The increased resistance increased in vitro performance of the device only at low air flow rate (30 l min^{-1}). Similar findings were demonstrated by Srichana et al. (1998) in testing formulations with dry powder inhalers having low, medium and high resistances between 30 and 90 l min^{-1} where the in vitro performance depended on device resistance only at low air flow rates. Further testing of the effect of air inlet size (Coates et al., 2006) at higher air flow rates resulted in either statistically insignificant or reduced in vitro performance. Decreasing air inlet size increased flow development time (time to develop specified air flow rate) and therefore the authors (Coates et al., 2006) demonstrated that large fraction of powder exited from the device prior to full flow and therefore a minimum fraction of the powder experienced the maximum turbulence levels leading to reduction in in vitro performance at higher air flow rates.

The studies described provided valuable insight into the impact of powder structure and device design on in vitro performance. It is not possible to define the major causes of powder de-agglomeration in a device, although the capsule aperture size has been shown to be important (Chew et al., 2002; Coates et al., 2005b). The outcomes of the studies described above provided an overview of the in vitro performance of a device in response to changing design parameters over the total powder emptying time. While these outcomes were important and help to understand the aerosolisation behaviour, the kinetics of cohesive powder behaviour may provide further insights into aerosolisation processes. Although, there were studies focusing on kinetics of de-agglomeration, they related to (a) de-agglomeration of particles in suspensions (Ding and Pacek, 2008), (b) non-cohesive particles of size range 250–1000 μm (De Villiers, 1997) or (c) carrier based dry powder formulation and focused on drug detachment from carrier surface (De Boer et al., 2004).

A recent study (Behara et al., 2011a) investigated the kinetics of emitted mass of single components (SS and LH300) by making use of laser diffraction particle sizing to compare three successful commercial devices of different designs and resistances of low (RH), medium (MI) and high [Handihaler® (HH)] (Clark and Hollingworth, 1993). The proposed study builds on this approach and examines the rate of de-agglomeration over the whole aerosolisation time for the three different devices above. The major purposes of this study were to develop a methodology for determining de-agglomeration *vs.* time profiles and to apply a numerical approach to estimate de-agglomeration rate constants. The study used SS and LH300 as model cohesive materials.

2. Materials and methods

2.1. Materials

The materials used in the current investigation were SS (Combrex Profarmaco, Milan, Italy) and LH300 (Borculoingredientsdomo, Borculo, The Netherlands). The volume median diameters ($n = 6$; mean ± sd) as determined by MasterSizer S were 3.4 ± 0.2 μm and 4.1 ± 0.1 μm respectively for SS and LH300. The primary size distributions of SS and LH300 are presented elsewhere (Behara et al., 2011c). RH (GSK, Middlesex, UK) and HH (Boehringer Ingelheim, Germany) were bought from a local pharmacy and MI was a kind donation from NanoMaterials Technology Pte Ltd., Singapore.

2.2. Initial processing of the materials

Micronised SS and LH300 samples were processed individually using a modified blending technique (Alway et al., 1996) prior to testing. 5 g batches of powder were prepared by placing in a glass bottle containing three ceramic beads (10 mm diameter) and shaken vigorously for a minute, and then tapped for 15 s to remove powder adhered to the corners. This process was repeated four times. The scanning electron micrographs of the processed materials shown in Fig. 1 demonstrated the cohesive nature of the materials.

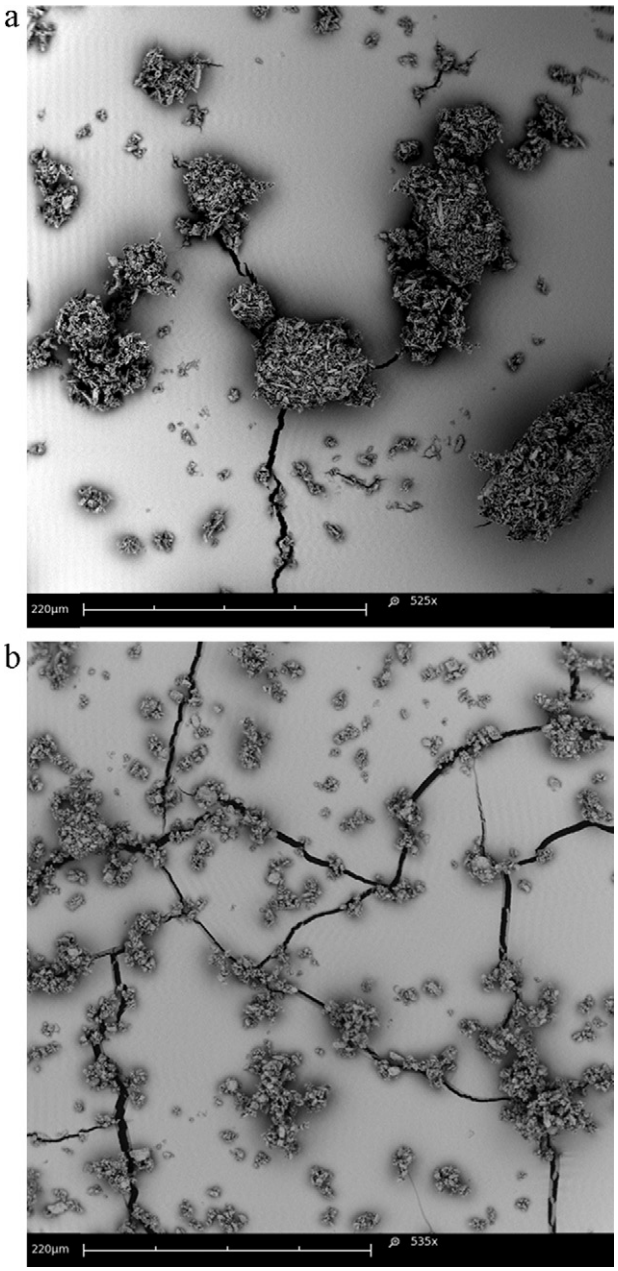

Fig. 1. Scanning electron micrographs of salbutamol sulphate (a) and lactohale 300 (b). The scale bar is 220 μm.

2.3. Aerosol cloud size distribution at specific time

The powders (SS and LH300) weighing 20 ± 1 mg were filled in gelatine no. 3 capsules (Capsugel, NSW, Australia) aerosolised horizontally through an inhalation cell of the Spraytec® (Malvern Instruments, Worcestershire, UK) at 30, 45, 60, 90, 120, 150 and 180 l min^{-1} for a period of 5 s using the RH and MI and 30, 45, 60, 90, 105 and 120 l min^{-1} using HH for 5 s to determine the particle size distributions of aerosolised powder. The measurements past 120 l min^{-1} could not be achieved with HH due to the capacity of the vacuum pump (HCP5, Copley Scientific Limited, Nottingham, UK). The horizontal distance between powder exit from the device to the laser beam was approximately 5 cm. The air flow rate was continuously monitored during dispersion using a digital flow-meter, DFM 2000 flow-meter (Copley Scientific Limited, Nottingham, UK) connected to the Spraytec and the opening and closing time of the solenoid valve was regulated by a critical flow controller TPK 2000 (Copley Scientific Limited, Nottingham, UK). Real time measurements were carried out at a data acquisition rate of 100 Hz (100 measurements per second) over a 5 s period. Data were collected using a 300 mm lens. Measurements were performed with data collection triggered manually. The measurements were made on five individual replicates of each material. Between the runs and prior to aerosolisation, the laser diffraction windows were cleaned until light energy was 20 units or less on detector number 1; the light energy tapers to a baseline value at detector number 36.

2.4. Statistical modelling and analysis

The cumulative emitted mass percent were modelled using a non linear least square regression analysis in the SigmaPlot 11.0 software (Systat Software, Inc., IL, USA). The statistical significance was carried out using one-way analysis of variance with Tukey's post hoc analysis and between the groups was carried out using independent sample *t*-test at a *p*-value of 0.05 using SPSS (version 17.0, SPSS, Inc., IL, USA).

3. Results and discussion

3.1. Particle size distributions of the aerosolised plume at various flow rates using different inhalers

The influence of air flow rate on the aerosolisation of micronised SS and LH300 was determined to measure the mean particle size distribution of the aerosolised plume from the three devices over the full aerosolisation time. In this manuscript, LH300 was used in the figures to illustrate specific behaviours; however, data for both LH300 and SS are summarised in tables and in the summary figures describing kinetic behaviour. The typical variability in the frequency *vs.* size distribution of the aerosolised plume of LH300 at 60 l min^{-1} is shown for RH, MI and HH in Fig. 2a. The variability seen at 60 l min^{-1} was typical of other air flow rates. The variability in size distributions with air flow rate was consistent with a previous study (Behara et al., 2011b). The mean frequency distributions of five replicates of LH300 at selected flow rates (45, 90 and 120 l min^{-1}) with the RH (Behara et al., 2011c), MI and HH are shown in Figs. 2b–d, respectively. The change in modal size and the frequencies of the fines, small and large agglomerates distributions for both SS and LH300 aerosolised with RH, MI and HH are presented in Table 1. For better visualisation and comparison, the standard deviations were not shown in Fig. 1b–d. However, the variability can be seen in Table 1.

For the RH, multimodal distributions were observed for the aerosolised plume with air flow rates of 45 l min^{-1} and above (Fig. 2b and Table 1). The Dv_{50} for fines mode did not change with increase in flow rate from 90 to 180 l min^{-1}, remaining around 7 μm with similar frequencies over the air flow rate range. In contrast, SS decreased from 10 μm at 90 l min^{-1} to about 3 μm at 180 l min^{-1} (Table 1) and the mean frequencies increased from 3.9% at 90 l min^{-1} to 4.7% at 180 l min^{-1}. In general, the small agglomerate modal size decreased with flow rate. For example, the small agglomerate modal size decreased from 136 μm at 60 l min^{-1} to 63 μm at 180 l min^{-1} with LH300, while the small agglomerate modal size decreased from 116.6 μm at 90 l min^{-1} to 85.8 μm at 180 l min^{-1} with SS. However, the change in small agglomerate modal size was least affected by air flow rate with SS powders. At very high flow rates (over 120 l min^{-1}), large agglomerates around 630–740 μm were observed with LH300 while no such agglomerates were observed with SS.

It was reported earlier that aerosolisation of both SS and LH300 with MI above 120 l min^{-1} resulted in capsule shattering (Behara

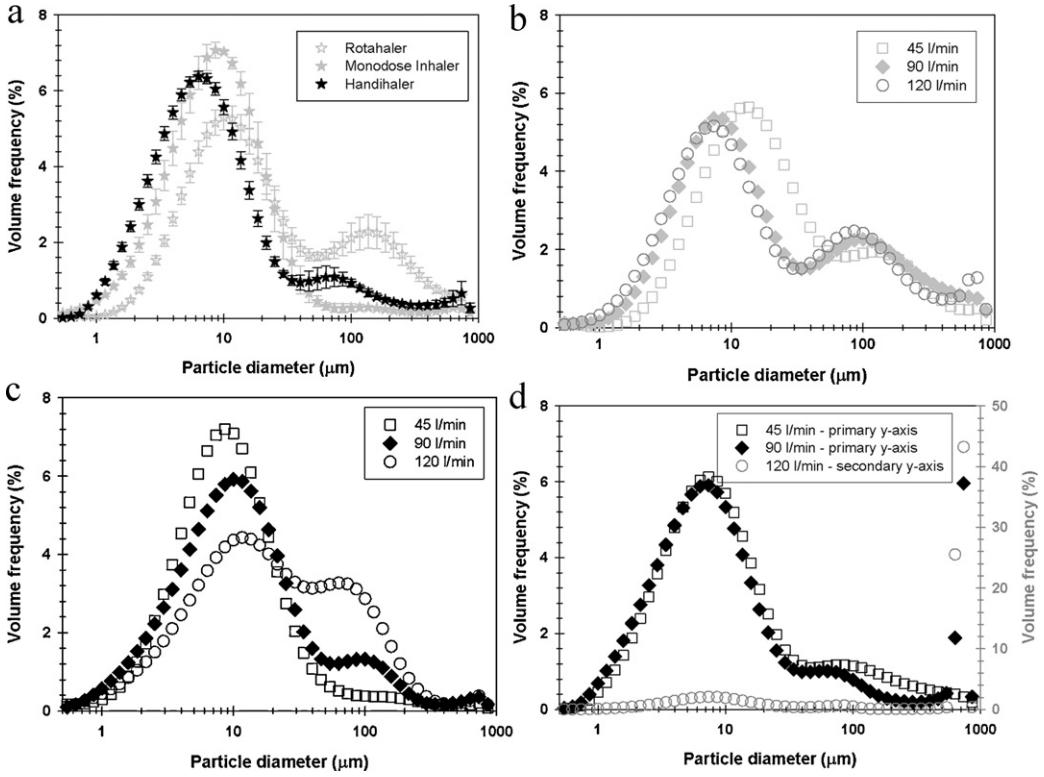

Fig. 2. Particle size distributions of aerosolised plume of lactohale 300 measured by laser diffraction and aerosolised from Rotahaler®, Monodose Inhaler® and Handihaler® at: (a) 60 l min^{-1} showing typical variability; the mean of five replicates of lactohale 300 aerosolised at 45, 90 and 120 l min^{-1} through (b) Rotahaler®, (c) Monodose Inhaler®, and (d) Handihaler® (120 l min^{-1} on secondary *y*-axis).

et al., 2011a). The influence of capsule shattering on the aerosolisation behaviour and resulting particle size distribution and therefore the de-agglomeration pattern was unknown. However, the presence or absence of capsule with AL (similar dispersion mechanism as MI) has been reported (Coates et al., 2005a) and the absence of capsule decreased particle-mouth piece impactions by 60% (Coates et al., 2005b). In addition, the absence of a capsule might change the fluid dynamics within the device and therefore the flow rates over 120 l min^{-1} aerosolised by MI were not considered further in this investigation. In contrast to the RH, the LH300 powders aerosolised by the MI (Fig. 2c) showed multimodal behaviour which developed as the air flow rate increased and thus the formation of small and

Table 1
Fines, small and large agglomerate modal sizes, and volume percent frequencies of salbutamol sulphate and lactohale 300 obtained from particle size distributions aerosolised by Rotahaler®, Monodose Inhaler® and Handihaler® ($n = 5$).

Device	Flow rate	Processed salbutamol sulphate						Processed lactohale 300					
		Fines		Small agglomerate		Large agglomerate		Fines		Small agglomerate		Large agglomerate	
		Dv_{50}	Fr.	Dv_{50}	Fr.	Dv_{50}	Fr.	Dv_{50}	Fr.	Dv_{50}	Fr.	Dv_{50}	Fr.
RH	30	85.8	6.8 ± 0.4	–	–	–	–	29.3	5.2 ± 0.7	–	–	–	–
	45	39.8	5.2 ± 0.4	–	–	–	–	13.6	5.6 ± 0.2	116.6	1.9 ± 0.3	–	–
	60	18.5	4.9 ± 0.3	Shoulder	–	–	–	10.0	5.3 ± 0.3	135.9	2.3 ± 0.5	–	–
	90	10.0	3.9 ± 0.4	116.6	3.5 ± 1.2	–	–	7.4	5.4 ± 0.6	100.0	2.3 ± 0.6	–	–
	120	5.4	4.0 ± 0.4	116.6	3.3 ± 1.0	–	–	7.4	5.2 ± 0.5	85.8	2.5 ± 0.8	735.6	1.3 ± 0.5
	150	4.0	4.4 ± 0.4	116.6	3.0 ± 1.0	–	–	7.4	4.3 ± 1.2	85.8	3.5 ± 1.4	631.0	2.4 ± 1.7
	180	3.4	4.7 ± 0.8	85.8	2.7 ± 0.8	–	–	7.4	5.0 ± 0.4	63.1	1.9 ± 0.7	631.0	4.6 ± 2.5
MI	30	18.5	4.6 ± 0.4	–	–	–	–	8.6	7.0 ± 0.2	–	–	–	–
	45	6.3	5.5 ± 0.4	–	–	–	–	8.6	7.2 ± 0.2	–	–	–	–
	60	4.6	6.1 ± 0.1	–	–	631.0	1.2 ± 0.3	8.6	7.1 ± 0.2	–	–	–	–
	90	4.6	6.2 ± 0.3	–	–	631.0	2.1 ± 1.3	10.0	6.0 ± 0.8	100.0	1.3 ± 1.0	735.6	0.4 ± 0.1
	120	4.0	5.8 ± 1.0	85.8	1.1 ± 0.8	631.0	2.4 ± 1.1	11.7	4.4 ± 0.3	63.1	3.3 ± 0.6	735.6	0.4 ± 0.2
	150	5.4	4.1 ± 0.4	73.6	3.0 ± 0.7	631.0	1.0 ± 0.3	15.9	3.4 ± 0.6	85.8	4.2 ± 1.0	735.6	1.4 ± 0.9
	180	6.3	4.3 ± 0.8	–	–	735.6	4.2 ± 3.0	–	–	73.6	5.3 ± 1.9	735.6	2.7 ± 1.9
HH	30	21.5	3.4 ± 0.2	–	–	–	–	8.6	5.3 ± 0.2	–	–	–	–
	45	4.6	3.8 ± 0.3	116.6	2.8 ± 0.6	–	–	7.4	6.1 ± 0.2	–	–	–	–
	60	3.4	4.9 ± 0.5	73.6	1.8 ± 0.6	–	–	6.3	6.4 ± 0.1	–	–	–	–
	90	3.4	5.2 ± 0.3	63.1	1.2 ± 0.3	630.1	3.6 ± 0.5	7.4	5.9 ± 0.5	–	–	735.6	6.0 ± 1.8
	105	3.4	3.2 ± 0.6	63.1	1.1 ± 0.4	735.6	29.4 ± 15.1	7.4	3.2 ± 0.6	63.1	1.2 ± 0.3	735.6	22.2 ± 10.3
	120	2.9	3.0 ± 0.6	85.8	0.6 ± 0.1	735.6	45.0 ± 15.2	7.4	2.1 ± 0.8	85.8	2.5 ± 0.8	735.6	43.2 ± 21.1

Flow rate, flow rate in l min^{-1}; Dv_{50} in μm; Fr., frequency in % presented as mean ± SD; RH, Rotahaler® (part of the data presented in Behara et al., 2011c); MI, Monodose Inhaler®; HH, Handihaler®.

large agglomerates was observed as the flow rate increased. The fines modal size increased from 8.6 μm at 30 l min^{-1} to 11.7 μm at 120 l min^{-1} (Table 1). In general, a similar pattern of behaviour was observed for the aerosolisation of SS with the formation of agglomerates observed at higher flow rates. In contrast to LH300, the fines mode size of SS decreased from 18.5 μm at 30 l min^{-1} to 4.0 μm at 120 l min^{-1}. The large agglomerate mode size (seen from 60 to 120 l min^{-1}) remained about 630 μm and its frequency also increased with air flow rate.

The HH did not operate in its normal manner at flow rates above 90 l min^{-1}. The capsule seemed to be stuck to the grid in the device and, as a result, the usual auditory signals due to capsule oscillation were not heard during its operation. Therefore the data over 90 l min^{-1} with both SS and LH300 was not considered further in this study. Using the HH, with LH300, the Dv_{50} of the fines mode was about 7–8 μm for full air flow rate range; the presence of large agglomerates was observed at 90 l min^{-1} (Fig. 2d and Table 1). Similar behaviour was noticed on aerosolisation of SS with the Dv_{50} of the fines mode decreasing from about 20 μm at 30 l min^{-1} to 3.4 μm at 90 l min^{-1}. However the mean large agglomerate modal size and standard deviation were higher with SS compared to LH300.

The differences in particle size distributions of LH300 between different devices could be attributed to differences in design which dictates the pressure drop across the device (Chew and Chan, 2001; Srichana et al., 1998; Chew et al., 2002; Chew and Chan, 1999). Apart from design, the mechanism of de-agglomeration also affected the particle size distribution patterns. It was demonstrated recently that the agglomerate break-up pattern depended on the structure of the powder bed (Behara et al., 2011b,c).

These mean particle size distributions provided a generalised overview when powders were aerosolised for a specific time and therefore showed an end point determination which did not provide any information on the kinetics of de-agglomeration. In order to understand the process of de-agglomeration and thus the kinetics of de-agglomeration, the change in particle size distributions at specific times were determined.

3.2. Particle size distributions profiles of lactohale 300 at a specific time with different inhaler devices

The particle size *vs.* frequency distributions of the aerosolised plume of LH300 at 45 l min^{-1} at given times of aerosolisation with RH, MI and HH are shown in Fig. 3a–c respectively. The specific times presented were 0.01 s (secondary *y*-axis for RH and HH), the times at which peak aerosol concentration were noticed [0.07, 0.71 (0.25 s was chosen since the value exceeded 0.5 s) and 0.29 s for RH, MI and HH respectively], 0.5, 1.0 and 2.0 s.

Aerosolisation of LH300 powders by RH at 45 l min^{-1}, resulted in a mono-modal distribution of agglomerates ($Dv_{50} \approx 185$ μm) at 0.01 s (Fig. 3a – secondary *y*-axis). From 0.07 s (the mean time to achieve peak concentration in the RH), the distributions were bi-modal (Fig. 3a – primary *y*-axis). The mean small agglomerate frequency gradually decreased from approximately 5 to 2% and moved to a smaller modal size (around 159 μm at 0.07 s to 117 μm at 2.0 s). The fines mean frequency increased (≈3% at 0.07 s to 6% at 2.0 s) and the fines mode remained about 14 μm. Similar trends were obtained at all air flow rates with both SS and LH300 aerosolised by RH.

The MI (Fig. 3b) has shown contrasting behaviour to RH on aerosolisation of LH300 at 45 l min^{-1}. In general, tri-modal distributions were noticed at all specific times. The small agglomerate mode decreased and then increased with time and ranged from approximately 100 to 250 μm, while fines mode increased from ≈6 μm at 0.01 s to 9 μm at 0.25 s where it remained constant. The patterns observed at 45 l min^{-1} were consistent with other air flow rates and also among both materials used in this investigation.

The LH300 powders aerosolised by HH have shown a mono-modal distribution with high frequency of agglomerates (around 250 μm) at 0.01 s (Fig. 3c – secondary *y*-axis). From 0.29 s (the mean time to achieve peak concentration), bi-modal distributions were seen and the small agglomerate modal size varied greatly with time and ranged from 86 to 250 μm (Fig. 3c – primary *y*-axis). Fines mode was not observed at 0.01 s; however, the modal size decreased from ≈9 μm at 0.29 s to 7 μm at 2.0 s. A slight improvement in fines means frequency was observed with increases in time. Similar characteristic particle size distributions resulted from SS and LH300 on aerosolisation at all air flow rates.

3.3. Profiles of volume percent less than 5.4 μm as a function of time for lactohale 300 powders

Using the particle size distributions, a measure of the extent of de-agglomeration (i.e., the percent of particles less than 5.4 μm) at specific time of aerosolisation for all materials and devices at all air flow rates was determined. The volume % less than 5.4 μm as a function of time for LH300 powders aerosolised by RH, MI and HH at 60 l min^{-1} demonstrates typical variability (Fig. 4a) and the mean volume % less than 5.4 μm at low (45 l min^{-1}), medium (90 l min^{-1}) and high (120 l min^{-1}) air flow rates for LH300 are shown in Fig. 4b and c for RH and MI respectively, and, 45 l min^{-1} and 90 l min^{-1} for HH in Fig. 4e. It should be noted that the data presented in Fig. 4 were the mean of all replicates but the data were truncated to the time when the aerosol concentration of one of the replicates (among five replicates) approached the base-line value.

At the start of aerosolisation (60 l min^{-1}), the variability in volume % less than 5.4 μm for LH300 was high for MI (Fig. 4a). The extent of de-agglomeration was highest with HH (about 45%) and lowest with RH (about 20%) at 60 l min^{-1}. The threshold in the extent of de-agglomeration was achieved rapidly with MI (Fig. 4a).

The de-agglomeration with RH approached a threshold with increase in time and the extent of de-agglomeration increased with air flow rate (Fig. 4b). The extent of de-agglomeration increased until 90 l min^{-1} above which similar extents of de-agglomeration were noticed. In contrast to LH300, SS powders aerosolised by RH showed continued increase in the extent of de-agglomeration with increases in air flow rate.

The aerosolisation of LH300 by MI rapidly achieved threshold extent of de-agglomeration levels (Fig. 4c). However, with increased air flow rate, decreased extents of de-agglomeration were noticed. At 120 l min^{-1}, the volume % less than 5.4 μm reached a threshold extent of de-agglomeration but then decreased with time. For SS powders aerosolised by MI, an increase in extent of de-agglomeration with air flow rate reached a threshold within 0.2 s at all air flow rates (Fig. 4d). At 120 l min^{-1}, once reaching the threshold extent of de-agglomeration, the volume % less than 5.4 μm decreased with air flow rate.

The volume % less than 5.4 μm *vs.* time profiles with HH (Fig. 4e) for aerosolised LH300 powders were similar to RH; except the time taken to reach threshold de-agglomeration levels which was short compared to RH. Similar volume % less than 5.4 μm *vs.* time profiles patterns were noticed with SS powders aerosolised by HH at all air flow rates.

3.4. Calculation of the cumulative fine particle mass

The cumulative fine particle mass can be calculated from the de-agglomeration profiles of volume % less than 5.4 μm *vs.* time profiles shown above. Firstly, the calculated emitted mass at specific times (EM_t) was obtained from the product of the fractional concentration at a specific times by the total emitted mass (Behara et al., 2011a). Secondly, the EM_t was multiplied by the fractional volume less than 5.4 μm at specific times to calculate the

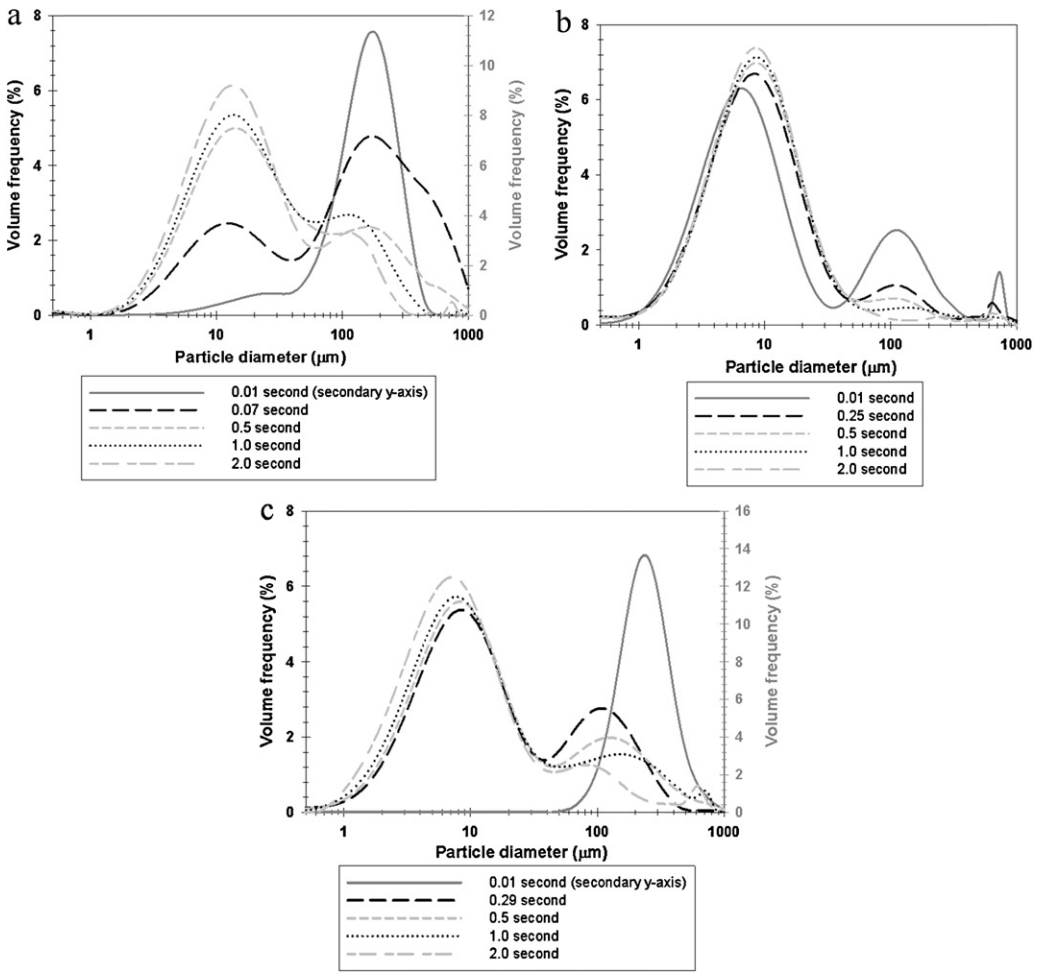

Fig. 3. The mean ($n = 5$) particle size distributions of aerosolised plume of lactohale 300 aerosolised at 45 l min^{-1} at a given time measured by laser diffraction and aerosolised from: (a) Rotahaler®, (b) Monodose Inhaler®, and (c) Handihaler®.

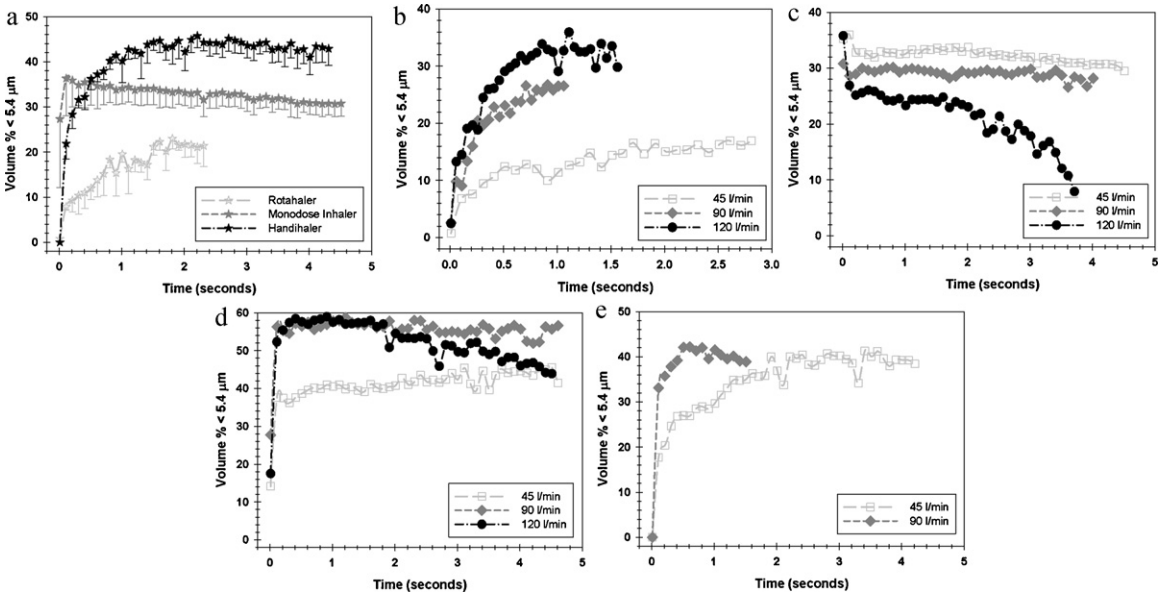

Fig. 4. Plots of volume % less than 5.4 μm as a function of time: (a) lactohale 300 aerosolised at 60 l min^{-1} from Rotahaler®, Monodose Inhaler®, and Handihaler® showing typical variability; mean ($n = 5$) volume % less than 5.4 μm for lactohale 300 at a given time aerosolised at 45, 90 and 120 l min^{-1} through: (b) Rotahaler®, (c) Monodose Inhaler® and, at 45 and 90 l min^{-1} through Handihaler® (e). Profile of Monodose Inhaler® for salbutamol sulphate (d) aerosolised at 45, 90 and 120 l min^{-1}.

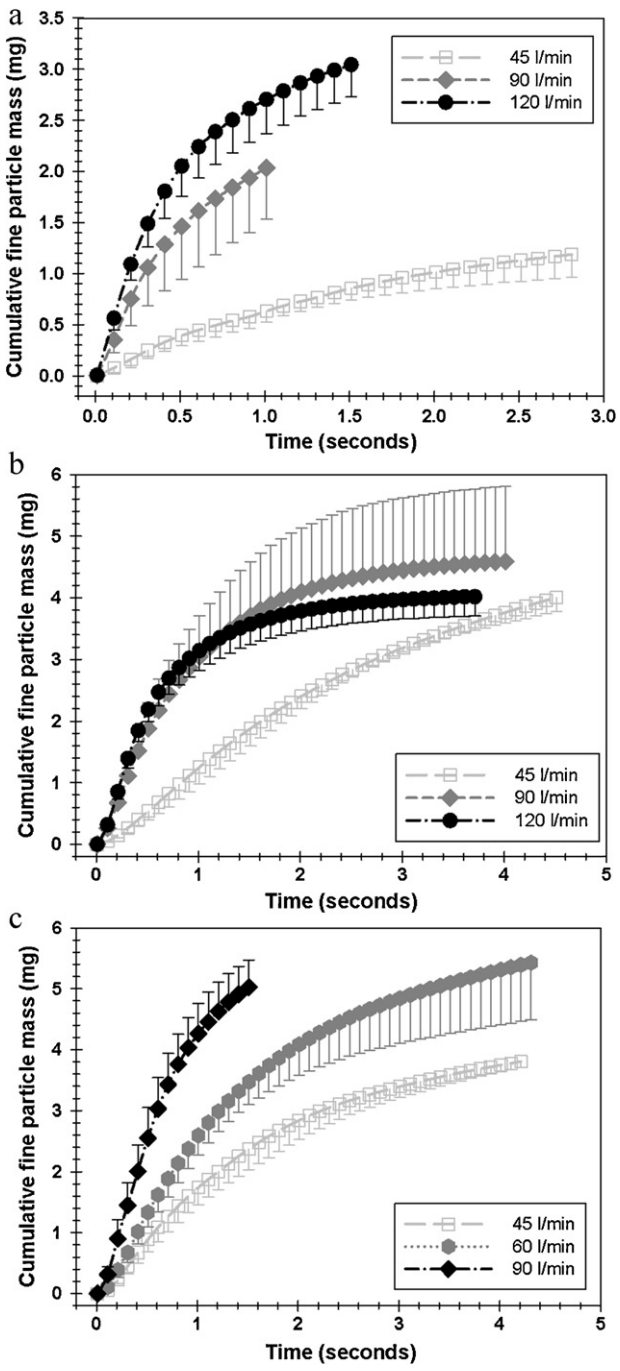

Fig. 5. Cumulative fine particle mass *vs.* time profiles for: (a) Rotahaler® and Monodose Inhaler®, (b) aerosolised at 45, 90 and 120 l min^{-1}, and (c) profiles of cumulative fine particle mass *vs.* time for Handihaler® aerosolised at 45, 60 and 90 l min^{-1} ($n = 5$; mean ± SD).

fractional fine particle mass (FPM_t), i.e., the mass of particles less than 5.4 μm at a specific time available for respiratory deposition. The cumulative fine particle mass ($CFPM_t$) was calculated and the $CFPM_t$ *vs.* time profiles for LH300 aerosolised from RH, MI at 45, 90 and 120 l min^{-1} and HH at 45, 60 and 90 l min^{-1} are presented in Fig. 5a–c respectively. The $CFPM_t$ *vs.* time profiles were different between devices; the time to reach maximum CFPM was lesser with RH compared to MI and HH. A clear difference in the extent of CFPM was observed between low and high air flow rates with all the devices. This behaviour is expected due to increased aerosolisation energy with increased air flow rate (Chew et al., 2002; Coates et al., 2005a).

3.5. Modelling the calculated cumulative fine particle mass ($CFPM_t$) vs. time profiles

In order to summarise the data in the $CFPM_t$ *vs.* time profiles, attempts were made to empirically model the data. All the $CFPM_t$ *vs.* time profiles of SS and LH300 aerosolised by three devices showed a gradual increase in CFPM with time (Fig. 5). There was no literature or theory to support the selection of a model to fit the data in Fig. 5. The shape of the plots suggested that a sigmoid or mono-exponential rise to maximum (MERM) model may be appropriate and the data were fitted to both equations. Both these models have parameters that relate to rate of de-agglomeration which was the focus of the current investigation. Therefore, the data were fitted with sigmoid (Eq. (1)) and MERM (Eq. (2)) equations as shown below.

$$CFPM_t = \frac{CFPM_{max}}{1 + e^{-(t - t_{0.5CFPM_{max}})/b}} \quad (1)$$

where '$CFPM_t$' is calculated cumulative fine particle mass, '$CFPM_{max}$' is the maximum calculated cumulative fine particle mass predicted by the model, 't' is the time, '$t_{0.5CFPM_{max}}$' is the time at which 50% maximum calculated cumulative fine particle mass occurs and 'b' is the difference in time between 0.75 and 0.25 of the maximum calculated cumulative emitted mass which is representative of the rate of calculated cumulative fine particle mass.

$$CFPM_t = CFPM_{max}(1 - e^{-k_d t}) \quad (2)$$

where '$CFPM_t$' is calculated cumulative fine particle mass, '$CFPM_{max}$' is the maximum calculated cumulative fine particle mass predicted by the model, 'k_d' is the rate of de-agglomeration to particles less than 5.4 μm and 't' is the time.

The non-linear least square data fitting to sigmoid (3 parameter) and MERM (2 parameter) for LH300 at 90 l min^{-1} between the three devices are presented in Table 2. Individual data replicates were fitted in order to get mean and standard deviations not only for the selection of the model but also to find the actual variability in the rate constant for de-agglomeration. The strategy for selection and comparison of the best fitting model using the fitting statistics in Table 2 as well as the non-linear least squares estimation of the equation parameters (Draper and Smith, 1981) have been described previously (Behara et al., 2011a,c). The coefficient of determination, norm and akaike information criteria (AIC) favoured the MERM as the most appropriate model compared to the sigmoid (Table 2). Similar goodness of fit statistics was obtained at all air flow rates for all the devices. However, the goodness of fit may be further improved by fitting the data to a higher order exponential fit. Thus, the fitting process was extended to bi-exponential rise to maximum 4 parameter (BERM) equation whose goodness of fit statistics are presented in Table 2.

Some of the replicates for the LH300 powders aerosolised by RH and MI did not converge with BERM while the dependencies for the HH data showed over-parameterisation. Therefore, the fitting process was continued with MERM. The MERM model did not converge with SS and LH300 powders at 30 l min^{-1} aerosolised through MI.

3.6. Influence of air flow rate on k_d for salbutamol and lactohale 300 powders

The rate constants of de-agglomeration, k_d, for SS and LH300 from modelling the data in Fig. 5 provided an understanding of the rates at which the devices de-agglomerate the materials. The influence of air flow rate on k_d for RH, MI and HH are presented in Fig. 6a and b respectively for SS and LH300. The k_d values for

Table 2
Modelling statistics for the fitting of replicates (lactohale 300 aerosolised at 90 l min^{-1}) of cumulative fine particle mass-time profiles for the Rotahaler®, Monodose Inhaler® and Handihaler® to sigmoid 3 parameter, mono-exponential rise to maximum 2 parameter and bi-exponential rise to maximum equations ($n = 5$; mean ± SD).

Model	Device	R^2	Norm	AIC	Dependencies				
					$x0$	a	b	c	d
Sigmoid (3P)	RH	0.9771 ± 0.0167	1.4 ± 0.6	6.5 ± 0.9	0.39 ± 0.12	0.58 ± 0.10	0.39 ± 0.07	n/a	n/a
	MI	0.9752 ± 0.0085	3.8 ± 0.9	8.6 ± 0.5	0.19 ± 0.02	0.35 ± 0.03	0.22 ± 0.02	n/a	n/a
	HH	0.9776 ± 0.0067	4.3 ± 1.6	8.8 ± 0.7	0.31 ± 0.07	0.48 ± 0.08	0.30 ± 0.06	n/a	n/a
Mono-exponential (2P)	RH	0.9908 ± 0.0083	1.1 ± 0.9	3.7 ± 1.5	n/a	0.83 ± 0.14	0.83 ± 0.14	n/a	n/a
	MI	0.9951 ± 0.0041	1.8 ± 1.4	4.8 ± 1.3	n/a	0.61 ± 0.10	0.61 ± 0.10	n/a	n/a
	HH	0.9915 ± 0.0020	2.5 ± 0.6	5.8 ± 0.4	n/a	0.83 ± 0.09	0.83 ± 0.09	n/a	n/a
Bi-exponential (4P)	RH	Some of the replicates did not converge							
	MI	Some of the replicates did not converge							
	HH	0.9919 ± 0.0026	2.6 ± 0.8	9.9 ± 0.6	n/a	1.00 ± 0.00	1.00 ± 0.00	1.00 ± 0.00	1.00 ± 0.00

3P, three parameter; 2P, two parameter; 4P, 4 parameter; RH, Rotahaler®; MI, Monodose Inhaler®; HH, Handihaler®; n/a, not applicable.

MI at 45 and 60 l min^{-1} are shown in grey since the data should be treated cautiously as a result of inability of the particle concentration in the aerosol plume to reach baseline concentrations from concentration *vs.* time profile presented elsewhere (Behara et al., 2011a). The k_d values for the powders aerosolised by MI at 30 l min^{-1} were not shown since the data did not converge. Some important observations are:

- Difference in k_d between devices: The k_d *vs.* air flow rate profiles for the various devices differed. In general, the k_d for RH were greatest and the k_d for the MI were lowest. However, the rate constant relationship depended on the material and air flow rate and more detailed comments on this relationship are presented as follows. For SS, the k_d for HH was significantly higher than those for the MI ($p \leq 0.002$), while no significance differences were observed with LH300 between air flow rates of 45–90 l min^{-1} ($p \geq 0.537$). No significant ($0.110 \leq p \leq 0.682$) differences were observed between RH and HH for LH300; however, for SS, significantly lower k_d values were demonstrated by HH compared with RH at 30 l min^{-1} ($p = 0.010$) and k_d values were higher with HH compared to RH at 60 l min^{-1} ($p = 0.012$). No significant differences ($0.118 \leq p \leq 0.372$) in k_d were observed between RH and MI for SS at 90, 120 l min^{-1} and LH300 at 45 and 90 l min^{-1}.
- Variability: RH showed high variability in k_d at all air flow rates with both SS and LH300. The variability in k_d with RH was higher than that of the MI or HH. MI showed lowest variability in k_d.
- Difference in k_d between air flow rates: In general, the k_d increased with increasing air flow rate. For RH, while an increasing trend in k_d values was observed, there was no significant difference ($p \geq 0.209$) in k_d between 45 and 180 l min^{-1} with SS, due to its large variability. Also, there was no significant differences in k_d values for LH300 between all the air flow rates ($p \geq 0.071$) except 45 l min^{-1} which was significantly lower ($p \leq 0.047$) compared to 150 and 180 l min^{-1}. For MI, k_d values significantly increased from 60 to 120 l min^{-1} with SS ($p \leq 0.008$) and LH300 ($p < 0.001$), but there was no significant difference in k_d with both SS ($p = 0.351$) and LH300 ($p = 0.852$) between 45 and 60 l min^{-1}. For HH, there was a significantly increased k_d value for SS with increased air flow rate ($p \leq 0.014$). However, no significant difference in k_d value was observed with 30 and 45 l min^{-1} for SS ($p = 0.388$) and LH300 ($p = 0.077$).
- Difference in k_d between powders: The profiles of k_d *vs.* air flow rate for the SS (Fig. 6a) and LH300 (Fig. 6b) for any given device showed patterns of behaviour. For RH, no significant differences in k_d ($0.077 \leq p \leq 0.786$) between materials were observed between 30 and 120 l min^{-1}; however at flow rates of 150 and 180 l min^{-1}, significant differences occurred. The large variability contributed to the inability to distinguish between the materials. For MI, the k_d was significantly different ($p < 0.004$) between materials only at 90 and 120 l min^{-1}; while for HH, the k_d was significant different ($0.018 \leq p \leq 0.001$) over flow rates of 30–90 l min^{-1}.

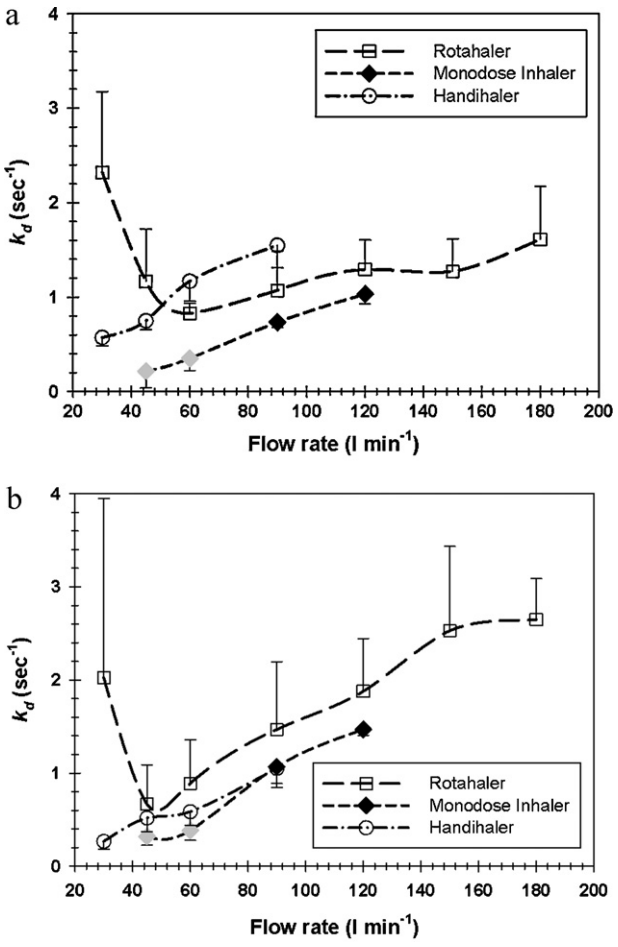

Fig. 6. The rate constant for cumulative fine particle mass as a function of flow rate profiles ($n = 5$; mean ± SD) aerosolised by Rotahaler®, Monodose Inhaler® and Handihaler® for salbutamol sulphate (a) and (b) lactohale 300. For MI aerosolised at 45 and 60 l min^{-1}, the data points are shown in grey.

The major mechanistic considerations from a passive capsule based dry powder inhalers involve factors related to device resistance, orientation and mode of action of capsule within the device including the exposure of powder in capsules to air (aperture size) and air flow rate.

The magnitude of k_d was not dependent of the resistance of the device. The device resistance to air flow as determined by differential pressure meter (Copley Scientific) were 0.015, 0.0222 and

0.0444 $(kPa)^{1/2}$ $(l\,min^{-1})^{-1}$ for RH, MI and HH respectively following the approach of Clark and Hollingworth (1993). In addition, the extent of de-agglomeration, represented by $CFPM_{max}$, was not related to device resistance. However, the magnitude of k_d was dependent on the size of the aperture in the capsule. The capsule aperture size for MI, HH and RH were 2.0, 3.0 and 10.4 mm, respectively. Decrease in capsule aperture size has been shown to increase powder de-agglomeration (Coates et al., 2005b; Chew et al., 2002). It was demonstrated (Chew et al., 2002) using a single device (DH) that the optimum capsule aperture size for high in vitro performance was between 1.00 and 2.38 mm. Coates et al. (2005b) showed, with AL, that capsule aperture size was more important in de-agglomeration rather than capsule aperture area, and that a decrease in capsule aperture size improved powder de-agglomeration by increasing powder–capsule impactions. In our current project, while the capsule aperture differs, the mode of action and mechanism within the device chamber are very different. Thus, the varying de-agglomeration rate constants is likely to be related, not only to capsule aperture size, but also the interaction of the air with the powder bed, the mechanism of operation of the device and device design, the residence time in the device and its influence on impactions.

The variability in rate constants was dependent on the mode of operation of the device. The capsule configuration within the device, including the volume of the device chambers was responsible for variability in k_d. Upon aerosolisation through the devices, the rotation or oscillation of the capsule was expected to be more uniform at a specific air flow rate with MI and HH due to the more controlled configuration and mode of action (spinning or oscillation) in small and constrained chambers of MI (2.78 ml) and HH (0.76 ml). With RH, after snapping the capsule base will be deposited in the capsule chamber and the capsule aperture will randomly orientate to air flow in the large chamber (11.58 ml). The chaotic movement and orientations in the capsule base prevented continuous interaction of air with the powder bed and was likely responsible for the large variability in the k_d seen for the RH in Fig. 6.

The magnitude of the k_d was generally dependent on the air flow rate for the MI and HH, but was not significantly different for the RH due to large variability associated. The aerosolisation energy (Chew et al., 2002) (with DH) and turbulent kinetic energy (with AL) of the flow field (Coates et al., 2005a) will increase with air flow rate leading to improved in vitro performance by increased number and intensity of impaction of agglomerates (Moreno et al., 2003; Thornton et al., 1999; Subero and Ghadiri, 2001; Samimi et al., 2003; Coates et al., 2005a). Therefore, increased k_d with increased air flow rate could be attributed to energy of the flow field (i.e., velocity and turbulent kinetic energy).

In general, the k_d were different for SS and LH300. The differences between the materials could be expected (Behara et al., 2011b,c) due to differences in powder structure (Fig. 1). The change in powder structure (Kendall and Stainton, 2001) will be associated with particle size, work of cohesion and packing fraction. However, the tensile strength of agglomerate within the powder bed follows log-normal (Veregin and Lam, 2003) distribution due to the existence of agglomerates with various extents of packing (Nichols et al., 2002). A recent study (Behara et al., 2011c) demonstrated that the relative de-agglomeration of SS was greater compared to LH300 due to the presence of non-dispersible agglomerates. Although this recent investigation could not provide evidence on whether powder structure was the cause for changes in k_d, it is evident from the current investigation that the powder structure has a affect on the kinetics of powder de-agglomeration.

The purpose of the current study was to develop methodology to experimentally determine the rate constant for de-agglomeration and was not to explore the fluid dynamic aspects between the devices and subsequent de-agglomeration mechanisms involved.

4. Conclusions

The study has developed a robust methodology to measure the kinetics of de-agglomeration during aerosolisation of cohesive powders from commercial inhaler devices. Cumulative fine particle mass *vs.* time profiles were obtained from the powder concentration, emitted mass and volume percent <5.4 μm, data which were embedded in the particle size distributions of the aerosol at specific times. Comparative cumulative de-agglomeration *vs.* time profiles showed exponential increases in de-agglomeration with time and non-linear least squares regression modelling estimated first order de-agglomeration rate constants, k_d. While the de-agglomeration capacity of a device for a particular set of conditions (air flow rate, material) could be determined by parameters such as emitted and fine particle dose, the de-agglomeration kinetics of devices could be best defined by the use of k_d. The k_d *vs.* air flow rate profiles were used to describe the relative rates of de-agglomeration between devices, the effect of air flow rate on de-agglomeration and comparison between materials. Large variability associated with RH was due to chaotic capsule orientation and volume of the capsule chamber. The de-agglomeration kinetics were found to be influenced by (a) the mode of operation of the devices including the extent of constrainment of the capsule, the relatively movement of the capsule and the size of the hole exposed to the air flow, (b) the air flow rate which was related to energy and (c) the material microstructural characteristics such as packing fraction, work of cohesion and particle size.

Previous studies have focussed on the extent of de-agglomeration defined by parameters such as fine particle fraction or fine particle dose. The significance of this study is that it provides a way to determine the rate of de-agglomeration and thus enhances the capability to understand the influence of device design, drug formulation and patient inspiration characteristics on optimising the delivery of drugs to the lungs.

Acknowledgements

Srinivas Ravindra Babu Behara is a recipient of Monash International Postgraduate Research Scholarship and Monash Research Graduate Scholarship. The authors would extend their thanks to Advent Pharmaceuticals Pty Ltd., BorculoIngredientsDomo and Capsugel for supplying salbutamol sulphate, lactohale 300 and gelatine capsules respectively and NanoMaterial Technology Pte Ltd., Singapore for providing MIs.

References

Alway, B., Sangchantra, R., Stewart, P.J., 1996. Modelling the dissolution of diazepam in lactose interactive mixtures. Int. J. Pharm. 130, 213–224.
Behara, S.R.B., Kippax, P., Larson, I., Morton, D.A.V., Stewart, P., 2011a. Kinetics of emitted mass—a study with three dry powder inhaler devices. Chem. Eng. Sci. 66, 5284–5294.
Behara, S.R.B., Kippax, P., Mcintosh, M.P., Morton, D.A.V., Larson, I., Stewart, P., 2011b. Structural influence of cohesive mixtures of salbutamol sulphate and lactose on aerosolisation and de-agglomeration behaviour under dynamic conditions. Eur. J. Pharm. Sci. 42, 210–219.
Behara, S.R.B., Larson, I., Kippax, P., Morton, D.A.V., Stewart, P., 2011c. An approach to characterising the cohesive behaviour of powders using a flow titration aerosolisation based methodology. Chem. Eng. Sci. 66, 1640–1648.
Chew, N.Y.K., Chan, H.K., 1999. Influence of particle size, air flow, and inhaler device on the dispersion of mannitol powders as aerosols. Pharm. Res. 16, 1098–1103.
Chew, N.Y.K., Chan, H.K., 2001. Use of solid corrugated particles to enhance powder aerosol performance. Pharm. Res. 18, 1570–1577.
Chew, N.Y.K., Chan, H.K., Bagster, D.F., Mukhraiya, J., 2002. Characterization of pharmaceutical powder inhalers: estimation of energy input for powder dispersion and effect of capsule device configuration. J. Aerosol Sci. 33, 999–1008.

Clark, A.R., Hollingworth, A.M., 1993. The relationship between powder inhaler resistance and peak inspiratory conditions in healthy volunteers—implications for in vitro testing. J. Aerosol Med. 6, 99–110.
Coates, M.S., Chan, H.K., Fletcher, D.F., Raper, J.A., 2005a. Influence of air flow on the performance of a dry powder inhaler using computational and experimental analyses. Pharm. Res. 22, 1445–1453.
Coates, M.S., Chan, H.K., Fletcher, D.F., Raper, J.A., 2006. Effect of design on the performance of a dry powder inhaler using computational fluid dynamics. Part 2. Air inlet size. J. Pharm. Sci. 95, 1382–1392.
Coates, M. S., Fletcher, D. F., Chan, H. K. & Raper, J. A., 2004a. A comparative study of two marketed pulmonary drug delivery devices using computational fluid dynamics. In: Dalby, R., Byron, P. R., Peart, J., Suman, J. D. & Farr, S. J. (Eds.), Respiratory Drug Delivery IX. California: Davis Healthcare International, River Grove, Illinois.
Coates, M.S., Chan, H.K., Fletcher, D.F., Raper, J.A., 2004b. Effect of design on the performance of a dry powder inhaler using computational fluid dynamics. Part 1. Grid structure and mouthpiece length. J. Pharm. Sci. 93, 2863–2876.
Coates, M.S., Chan, H.K., Fletcher, D.F., Raper, J.A., 2005b. The role of capsule on the performance of a dry powder inhaler using computational and experimental analyses. Pharm. Res. 22, 923–932.
De Boer, A.H., Hagedoorn, P., Gjaltema, D., Lambregts, D., Irngartinger, M., Frijlink, H.W., 2004. The rate of drug particle detachment from carrier crystals in an air classifier-based inhaler. Pharm. Res. 21, 2158–2166.
De Villiers, M.M., 1997. Description of the kinetics of the deagglomeration of drug particle agglomerates during powder mixing. Int. J. Pharm. 151, 1–6.
Ding, P., Pacek, A.W., 2008. De-agglomeration of silica nanoparticles in the presence of surfactants. J. Dispersion Sci. Technol. 29, 593–599.
Draper, N.R., Smith, H., 1981. Applied Regression Analysis. John Wiley & Sons, New York.
Kendall, K., Stainton, C., 2001. Adhesion and aggregation of fine particles. Powder Technol. 121, 223–229.
Moreno, R., Ghadiri, M., Antony, S.J., 2003. Effect of the impact angle on the breakage of agglomerates: a numerical study using DEM. Powder Technol. 130, 132–137.
Nichols, G., Byard, S., Bloxham, M.J., Botterill, J., Dawson, N.J., Dennis, A., Diart, V., North, N.C., Sherwood, J.D., 2002. A review of the terms agglomerate and aggregate with a recommendation for nomenclature used in powder and particle characterization. J. Pharm. Sci. 91, 2103–2109.
Samimi, A., Ghadiri, M., Boerefijn, R., Groot, A., Kohlus, R., 2003. Effect of structural characteristics on impact breakage of agglomerates. Powder Technol. 130, 428–435.
Srichana, T., Martin, G.P., Marriott, C., 1998. Dry powder inhalers: the influence of device resistance and powder formulation on drug and lactose deposition in vitro. Eur. J. Pharm. Sci. 7, 73–80.
Steckel, H., Muller, B.W., 1997. In vitro evaluation of dry powder inhalers. 1. Drug deposition of commonly used devices. Int. J. Pharm. 154, 19–29.
Subero, J., Ghadiri, M., 2001. Breakage patterns of agglomerates. Powder Technol. 120, 232–243.
Thornton, C., Ciomocos, M.T., Adams, M.J., 1999. Numerical simulations of agglomerate impact breakage. Powder Technol. 105, 74–82.
Veregin, R.P.N., Lam, M., 2003. Measurement of cohesive force distributions in powder flow: the effect of metal oxide surface additives on xerographic toner. J. Imaging Sci. Technol. 47, 418–423.
Visser, J., 1989. van der Waals and other cohesive forces affecting powder fluidization. Powder Technol. 58, 1–10.
Voss, A., Finlay, W.H., 2002. Deagglomeration of dry powder pharmaceutical aerosols. Int. J. Pharm. 248, 39–50.